Dynamics of Odor Representation in Locust Olfactory System

An End-Semester Report

Saptarshi Soham Mohanta (20171096)

September 2019

Abstract

The Locust Olfactory System has three main stages of Odor Representation: detection by the Olfactory Receptor Neurons (ORNs), spatiotemporal coding by the Antennal Lobe (AL), and reliable odor identity representation in the Mushroom Body (MB). Previous theoretical studies have proposed a model of odor representation via activation of sub-networks of *all* AL neurons which leads to spatiotemporal patterning. This pattern of activity then converges on the Mushroom Body, giving us an identity readout. We propose an alternate idea in which the network structure of the AL gives rise to a dynamical system with a large number of attractors and the activity of a sub-network of PNs acts as a director of the activity on odor onset. We also suggest that the fixed point representation of odors in the trajectories of the activity space may reflect this in the activity. We try to build a scaled-down model of the complete locust olfactory system and study the dynamics of the odor representations with realistic ORN activity, a physiological model of AL and dynamic MB activity as a readout.

1 Introduction

Understanding the basis and dynamics of stimulus-map generation and stimulus-coding in neural circuitry[19] has always been a topic of interest to a large number of people in the neuroscience community and has been substantiated via a large body of experiment and theoretical work[6, 21, 33]. The olfactory system has thus emerged as a prominent model in neuroscience.[14, 5] The study of function and organization of olfactory systems across different species has allowed the community to gain further insight into how animals are capable of detection, encoding, and processing of olfactory stimuli allowing them to perform complex tasks such as odor discrimination and odor association.[2, 7]

Finding a mate or food source for an insect is chiefly an olfactory process for insects which involves the reliable detection, representation, and recognition of an odor stimulus in the presence of a complex dynamic and turbulent background.[27] Insects have evolved highly efficient olfactory systems to detect ecologically relevant odorants with very high sensitivity in order to decode the olfactory signals to lead to relevant behaviors.[18]

This form of coding requires an internal and external representation of information. Each odorant carries a characteristic combination of simple (or primary) stimuli. Internally, the characteristic pattern of the stimulus molecules must be transformed into a patterned neural discharge which somehow reflects the specificity of the input signal from the odorous molecules. However, this process does not happen over a single layer of processing. The input is transformed over successive levels of the sensory system and undergoes multiple steps of processing to give an output that is a reliable representation of the input stimulus. [34]

In the Insect Olfactory system, the olfactory processing happens over multiple levels (Fig 1.A): Odorant detection at the Olfactory Receptor Neurons (ORNs), the generation of a reliable spatiotem-

poral code in the Antennal Lobe (AL), and representation of odor identity in the Mushroom Body (MB).[9] Previous experimental and theoretical studies[23, 24, 32, 13, 3, 4, 22] have revealed a lot of details about the locust olfactory system particularly the Locust Antennal Lobe where a network of excitatory PNs and inhibitory interneurons interact on odor detection to create a spatiotemporal pattern which is representative of an odor at a specific concentration.

The current idea of how the coding of odor information occurs in the AL is based majorly on the study of the in-vivo activity of the PNs and LNs and the modeling of this network phenomenon [3, 4, 31, 25, 22] with Hodgkin-Huxley neurons based on fits from electrophysiology data. This approach has helped explain many properties of the network behavior but is based on simplifying assumptions that may not stand in the real system. Most studies of the AL [31, 3, 4, 22], assumes what we call a model of "subnetwork selection"(Fig 1.B) which involved similarly structured spatially pattern input to a subset of both LNs and PNs (thus the name) that leads to the formation of a spatiotemporal pattern driven by the interaction of the set of projection neurons and local interneurons that were activated.

However, the form of input required for such a model may not be realistic. Experimental and theoretical studies of ORNs and their connectivity to the AL have revealed that not only is the behavior of the ORNs very diverse[25, 11, 10] but the connectivity patterns are widely different between LNs and PNs [25, 13, 8, 15, 17]. Particularly, LNs have a much larger dendritic arborization[15] than the PNs and thus are more likely to show broad and similar activation in almost all LNs on odor onset. There is also evidence that the diversity of PNs may help understand the diversity in PN activity that is absent in the "sub-network selection" model.

Also, it has previously been shown that the representation in the olfactory system follows a fixed point like representation along with transient dynamics in both experimental and theoretical paradigms.[19, 31, 22] Not many studies[31] have tried to study the dynamics of the fixed point representation across different layers and find the driving forces for determining the fixed point for odor representations in the different levels of the olfactory circuit. The fixed point approach may be a handy tool as it may reveal information about how the information is coded spatiotemporally or help determine the driving forces for the dynamics.

2 Problem Statement

We aim to consolidate the well-studied model of the Locust Antennal Lobe with the diversity of the ORN responses as observed in-vivo in the Locust and the realistic connectivity patterns between the ORNs and AL to build a coherent model of Locust Olfaction. These changes include dimorphic classes of responses, firing rate adaptation, and inhibitory responses in ORNs and difference in connectivity patterns of PNs and LNs.[25] On an average, PNs receive input from a small fraction of all ORN cell types which converge to the same glomeruli[8, 13] while LNs receive input from a significant fraction of all ORNs due to their large dendritic arbors[15]. This connectivity means that there is a more precise representation of the identity of the active ORNs in the input to the PNs and not the LNs which receive broad and similar responses across neurons.

The introduction of these parameters, no doubt pushes us to change our current idea of how the AL generates the spatiotemporal code. We propose a new alternative model that takes into account these new parameters which we call the 'activation driven attractor model.'(Fig 1.B) We propose that the Antennal Lobe connectivity pattern particularly the LNs, which are interconnected to each other by direct inhibitory connections and indirect excitatory connections, on activation generate a system of attractors states which depends on the structure of the network. The number of attractor states that this network may have is potentially enormous, but in the absence of a strong driving tendency, the attractor state reached on activation would be stochastic. We propose that the identity of ORNs that is encoded in the input to the PNs acts as this driving force. The system is driven to an attractor in the LNs circuit that is representative of the odor identity by the influence of the active PNs. Once such an attractor has been reached, the PN activity gets entrained to the LN activity.

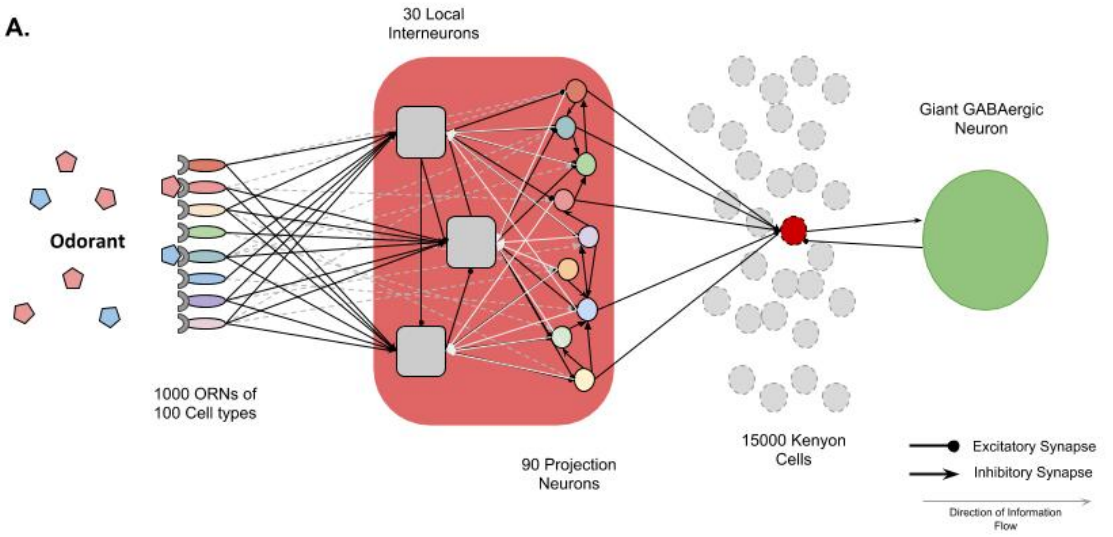
A.
30 Local Interneurons
Odorant
1000 ORNs of 100 Cell types
90 Projection Neurons
15000 Kenyon Cells
Giant GABAergic Neuron
Excitatory Synapse
Inhibitory Synapse
Direction of Information Flow

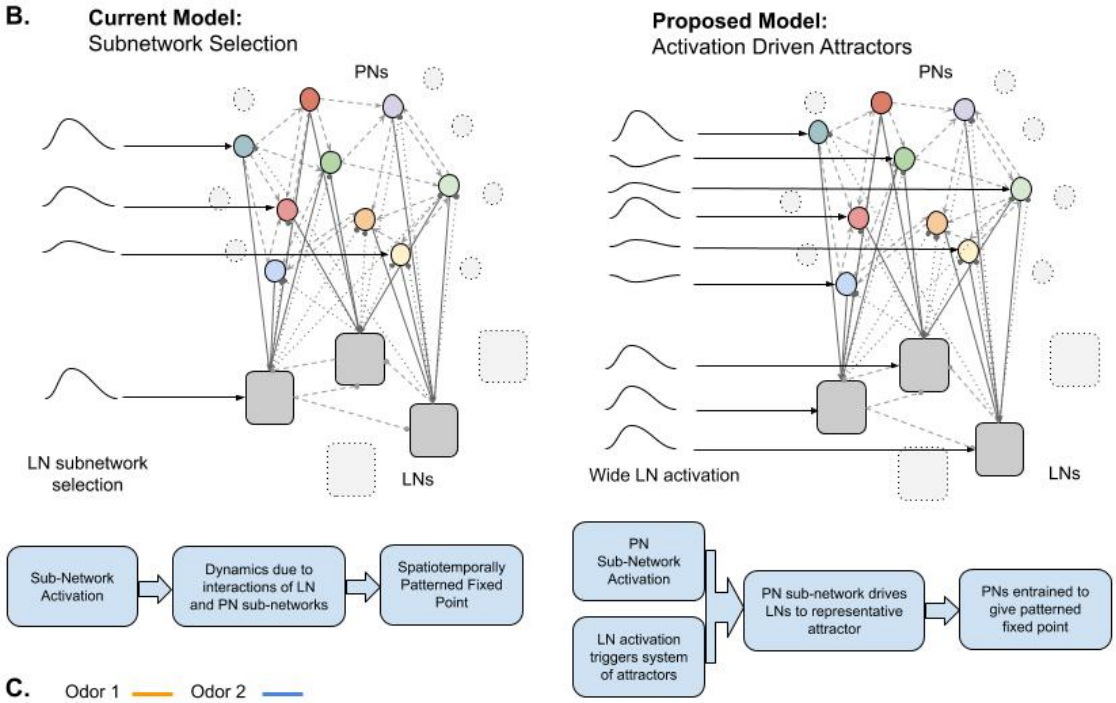
B.
Current Model:
Subnetwork Selection
PNs
LN subnetwork selection
LNs
Sub-Network Activation
Dynamics due to interactions of LN and PN sub-networks
Spatiotemporally Patterned Fixed Point
Proposed Model:
Activation Driven Attractors
PNs
Wide LN activation
LNs
PN Sub-Network Activation
LN activation triggers system of attractors
PN sub-network drives LNs to representative attractor
PNs entrained to give patterned fixed point

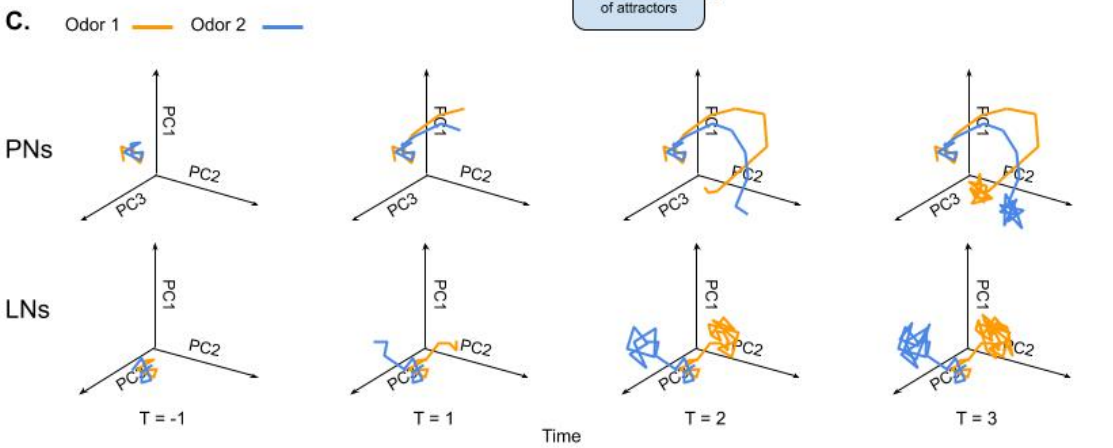
C.
Odor 1
Odor 2
PNs
LNs
PC1
PC2
PC3
T = -1
T = 1
T = 2
T = 3
Time

Figure 1: Objectives of the project (A) A schematic of the Locust Olfactory System from the Olfactory Receptor Neurons on the Antenna and Maxillary Palps, the Projection Neurons and Local Interneurons in the Antennal Lobe, Kenyon Cells in the Mushroom Body and the Giant GABAergic Neuron in the Mushroom Body calyx (B) Models of Patterning in the Locust AL: Current model of subnetwork selection contrasted with our proposed model of activation driven attractors (C) Signature of our new proposed model in the fixed-point representation of the dynamical system. (T=-1) Baseline Activity, (T=1) PNs show quick-change activity and LNs move rapidly towards attractor state represented by a fixed point, (T=2) LNs settle at a fixed point, PNs approach fixed point entrained by the LN activity, (T=3) PNs completely entrained to give fixed point

In the activity space of the LNs and PNs, these attractor states may appear as fixed points or limit cycles.[19, 22, 25, 32] We propose that we may be able to see evidence of our model in the activity space dynamics.(Fig 1.C) Finally, since at the end of olfactory processing, a readout of odor identity is required, we also supplement the AL activity with a dynamically inhibited Mushroom Body model.[31, 12] This helps us see at which stage of the olfactory processing is the odor discrimination reliable and how the AL dynamics play a role in the representation of odor identity in the MB.

3 Approach

The 3-Level Neuronal Pathway

In order to probe the question that this project proposes, we build a scaled down model of the locust olfactory system (Fig 1.A) that consists of 100 ORNs cell types with 10 replicates of each type[25] ($\sim$150 cell types in-vivo[16]), 90 Cholinergic Projection Neurons ($\sim$900 neurons in-vivo), 30 GABAergic (fast and slow) LNs ($\sim$300 neurons in-vivo), 15000 Kenyon Cells ($\sim$50000 in-vivo)[31] and 1 Giant GABAergic Neuron (1 in-vivo). The connectivity patterns are based on limited experimental estimates. PNs receive input from 5% of all ORN cell types all replicates of which converge towards the same PNs.[8] LNs on the other hand receive input from 70% of all ORNs.[15] Since there is no clear evidence of stereotyped network connectivity in the Locust AL, we assume probabilistic connections. The probabilities are set as $P(PN \rightarrow PN) = 0.5$,$P(PN \rightarrow LN) = 0.5$,$P(LN \rightarrow PN) = 0.5$, and $P(LN \rightarrow LN) = 0.5$.[3, 4, 31] Experimental data seems to suggest each KC receives input from a large fraction of all PNs compared to what is observed in *D. melanogaster* ($\sim$5% of all PNs) which we take to be $\sim$30% of all PNs.[31, 12]

ORN Model

For our model of the ORN, we use a firing rate based model (Fig 2.A) based on the experimental data and model proposed by Raman et. al.[25] The firing rate response of each ORN in this model to any given odorant was fully characterized a set of parameters: Peak Firing Rate @ 20 Hz, Baseline Firing Rate @ 4 Hz, latency of odor response Uniform(0,200) ms, rise time constant Uniform(0,600) ms, fall time constant Uniform(0,1200) ms, adaptation time constant Uniform(0,1200) ms, adaptation extent Uniform(1.0,0.5), response tuning coefficient Uniform(0.66,5) and Maximum Response Amplitude (between baseline firing rate and maximum firing rate). These parameter values were chosen based on recordings from ORNs.[25, 10]

Each odorant is represented as a vector ($\overrightarrow{Odor}$) in an (n=2)-dimensional space (can be interpreted as the first n PCs of chemical properties of the odorant)[26], where the magnitude of the vector is a proxy for the concentration of the odorant. We take unit magnitude as the maximum concentration of the odorant. Other than the above parameter, each ORN also has a receptive field vector ($\overrightarrow{ORN_i}$) which is a random unit vector on (n=2)-dimensions.

Given $\sigma(x) = \frac{1}{1+e^{-a_1(x-a_2)}}$ with $a_1 = 15$,$a_2 = 15$ and $\theta_{\overrightarrow{x_1}\overrightarrow{x_2}}$ is the angle between $\overrightarrow{x_1}$ and $\overrightarrow{x_2}$. The relative max response over baseline is given by

$$R_i = (1 - \frac{baseline}{firing}) \times \sigma\big(|\overrightarrow{Odor}| \times \cos{(\theta_{\overrightarrow{ORN_i}\overrightarrow{Odor}})}^{tuning}/2\big)$$

if $\theta_{\overrightarrow{Odor}\overrightarrow{ORN_i}}$ <inhibition threshold which we set as 164 degrees else the ORN is inhibited completely and

$$R_i = -\frac{baseline}{firing}$$

To simulate the dimorphic behavior of ORN response (Fig 2.A) [10, 25], each ORN could either be a sharp response ORN or a Broad Response ORN with equal probability. For the sharp response ORNs, on odorant stimulation, after the initial latency period increased from its relative baseline firing rate to relative max response over baseline with its rise time constant (τ_{rise}) according to the functional form $t \times e^{-\frac{2t}{\tau_{rise}}},\ 0 < t < \tau_{rise}$. and after that the response would fall with time constant τ_{fall} to relative baseline firing rate with the functional form $e^{-\frac{t}{t_{fall}}},\ 0 < t < \infty$. For broad response ORNs, similarly after the initial latency period increased from its relative baseline firing rate to relative max response over baseline with its rise time constant (τ_{rise}) according to the functional form $t \times e^{-\frac{t}{\tau_{rise}}},\ 0 < t < \tau_{rise}$. and following that the response would fall with time constant τ_{adapt} to adaptation extent times relative max response over baseline with the functional form $e^{-\frac{t}{t_{adapt}}},\ 0 < t <$time to odor offset. Finally the response would fall with time constant τ_{fall} to relative baseline firing rate with the functional form $e^{-\frac{t}{t_{fall}}},\ 0 < t < \infty$. Finally all responses are converted to actual firing rates by multiplying with the peak firing rate.

This model generates the firing rate response of various odors with relative degrees of similarity which we can use combine at the postsynaptic end in the AL to give us a proxy for conductance changes for acetylcholine induced channels in the post-synaptic neurons. We can add some random gaussian noise to the current input for the AL to simulate experimental noise and stochastic firing. One alternative that can be explored is to use the firing rate profiles to generate spike trains which can be combined convolved with a linearly decreasing kernel to give a more accurate representation of postsynaptic current to ALs.

AL Model

For simulating the Locust Antennal lobe, we construct our model based on Bazhenov, 2001 [3]. Locust AL has two types of neurons. Inhibitory Local Interneurons (LN) produce GABAergic Synapses, ie. GABAa (Fast) and Metabotropic GABA (Slow).[3, 4] They synapse onto other Local Interneurons and to Projection Neurons. Projection Neurons (PN) produce Cholinergic Synapses, ie. Acetylcholine. They synapse onto local interneurons and also project to the mushroom body outside the AL and act as the output for the AL.

In our model, the neurons are modelled to have a hodgkin huxley dynamics. PNs express voltage-gated Na^+ channels, voltage-gated K^+ channels, transient K^+ channels, and general leak channel. Thus. the dynamics for the PN as described by the equation:

$$C_m \frac{dV_{PN}}{dt} = I_{stim} - I_L - I_{Na} - I_K - I_A - I_{GABA_a} - I_{GABA_b} - I_{Ach}$$

where

$$I_L = g_L(V - E_L),\ g_L = 0.3,\ \mu S\ E_L = -64\ mV$$
$$I_{Na} = g_{Na} m_{Na}^3 h_{Na}(V - E_{Na}),\ g_{Na} = 7.15\ \mu S,\ E_{Na} = 50\ mV$$

$$I_A = g_A m_A^4 h_A (V - E_A),\ g_A = 1.43\ \mu S,\ E_A = -95\ mV$$
$$I_K = g_K n_K^4 (V - E_K),\ g_K = 3.6\ \mu S,\ E_K = -95\ mV$$

For potassium channel:

$$T = 23°C,\ \phi = 3.0^{(T-36.0)/10},\ V' = V - (-50)$$
$$\alpha_n = 0.02\frac{15.0 - V'}{e^{(15.0-V')/5.0} - 1.0},\ \beta_n = 0.5e^{(10.0-V')/40.0}$$
$$t_n = 1.0/((\alpha_n + \beta_n)\phi),\ n_\infty = \alpha_n/(\alpha_n + \beta_n)$$
$$\frac{dn_k}{dt} = -\frac{1}{tn}(n_K - n_\infty)$$

For sodium channel:

$$T = 23°C,\ \phi = 3.0^{(T-36.0)/10},\ V' = V - (-50)$$
$$\alpha_m = \frac{0.32(13.0 - V')}{e^{(13.0-V')/4.0} - 1.0},\ \beta_m = \frac{0.28(V' - 40.0)}{e^{(V\_40.0)/5.0} - 1.0}$$
$$\alpha_h = 0.128e^{(17.0-V')/18.0},\ \beta_h = \frac{4.0}{e^{(40.0-V')/5.0} + 1.0}$$
$$t_m = 1.0/((\alpha_m + \beta_m)\phi),\ m_\infty = \alpha_m/(\alpha_m + \beta_m)$$
$$t_h = 1.0/((\alpha_h + \beta_h)\phi),\ h_\infty = \alpha_h/(\alpha_h + \beta_h)$$
$$\frac{dm}{dt} = -\frac{1}{tm}(m - m_\infty),\ \frac{dh}{dt} = -\frac{1}{th}(h - h_\infty)$$

For transient potassium channel:

$$T = 23°C,\ \phi = 3.0^{(T-23.5)/10}$$
$$m_\infty = \frac{1.0}{1.0 + e^{-(V+60.0)/8.5}},\ h_\infty = \frac{1.0}{1.0 + e^{(V+78)/6.0}}$$
$$t_m = \frac{1.0}{e^{(V+35.82)/19.69} + e^{-(V+79.69)/12.7} + 0.37}$$
$$t_h = \frac{1.0}{(e^{(V+46.05)/5.0} + e^{-(V+238.4)/37.45})\phi}, when\ V < -63\ mV else = 5.1$$
$$\frac{dm}{dt} = -\frac{1}{tm}(m - m_\infty),\ \frac{dh}{dt} = -\frac{1}{th}(h - h_\infty)$$

Unlike the Projection neuron, the local interneurons do not have the normal sodium-potassium channel action potentials. They expresse voltage-gated Ca^{2+} channels, voltage-gated K^+ channels, Calcium-dependent K^+ channels, and general leak channel. Here, opposite interactions between K and Ca channels cause longer extended action potentials. The dynamics in intracellular Ca^{2+} causes changes in K(Ca) channel dynamics allowing for adaptive behavior in the neurons. Thus Local Interneurons have a dynamics somewhat similar to traditional Na-K Hodgkin Huxley model as described below:

$$C_m \frac{dV_{LN}}{dt} = -I_{stim} - I_L - I_{Ca} - I_K - I_{K(Ca)} - I_{GABA_a} - I_{Ach}$$

where

$$I_L = g_L(V - E_L),\ g_L = 0.3\ \mu S,\ E_L = -50\ mV$$
$$I_K = g_K n_K^4 (V - E_K),\ g_K = 36\ \mu S,\ E_K = -95\ mV$$

$$I_{Ca} = g_{Ca} m_{Ca}^2 h_{Ca} (V - E_{Ca}),\ g_{Ca} = 5\ \mu S,\ E_{Ca} = 140\ mV$$

$$I_{K(Ca)} = g_{K(Ca)} m_{K(Ca)} (V - E_A),\ g_{K(Ca)} = 0.045\ \mu S, E_{K(Ca)} = -90\ mV$$

For potassium channel:

$$T = 23°C,\ \phi = 3.0^{(T-36.0)/10},\ V' = V - (-50)$$

$$\alpha_n = 0.02 \frac{15.0 - V'}{e^{(15.0-V')/5.0} - 1.0},\ \beta_n = 0.5 e^{(10.0-V')/40.0}$$

$$t_n = 1.0/((\alpha_n + \beta_n)\phi),\ n_\infty = \alpha_n/(\alpha_n + \beta_n)$$

$$\frac{dn_k}{dt} = -\frac{1}{tn}(n_K - n_\infty)$$

For calcium channel:

$$m_\infty = \frac{1.0}{1.0 + e^{-(V+20.0)/6.5}},\ h_\infty = \frac{1.0}{1.0 + e^{(V+25.0)/12}}$$

$$t_m = 1.5,\ t_h = 0.3 e^{(V-40.0)/13.0} + 0.002 e^{(60.0-V)/29}$$

$$\frac{dm}{dt} = -\frac{1}{tm}(m - m_\infty),\ \frac{dh}{dt} = -\frac{1}{th}(h - h_\infty)$$

For calcium dependent potassium channel:

$$\alpha_m = 0.01[Ca^{2+}],\ \beta_m = 0.02$$

$$t_m = 1.0/((\alpha_m + \beta_m)),\ m_\infty = \alpha_m/(\alpha_m + \beta_m)$$

$$\frac{dm_{K(Ca)}}{dt} = -\frac{1}{tm}(m_{K(Ca)} - m_\infty)$$

For calcium dynamics:

$$\frac{d[Ca^{2+}]}{dt} = -A_{Ca} I_{Ca} - \frac{Ca - Ca_\infty}{\tau_{Ca}}$$

$$A_{Ca} = 2 \times 10^{-4}\ \frac{mMcm^2}{ms\mu A}$$

$$Ca_\infty = 2.4 \times 10^{-4}\ mM$$

$$\tau_{Ca} = 150\ ms$$

Finally, we also setup equations for the synapses which are given by hodgkin-huxley like gating characteristics for cholinergic and fast GABAa synapses:

$$I_{syn} = g_{syn}[O](V - E_{syn})$$

$$\frac{d[O]}{dt} = \alpha(1 - [O])[T] - \beta[O]$$

For cholinergic synapses:

$$E_{ach} = 0mV,\ A = 0.5,\ t_{max} = 0.3ms,\ t_{delay} = 0.0,\ \alpha = 10ms^{-1},\ \beta = 0.2ms^{-1}$$

$$[T] = A\theta(t_{max} + t_o + t_{delay} - t)\theta(t - t_o - t_{delay}))$$

with $g_{ach} = 0\mu S$ between PNs, i.e. no PN-PN connection, and $g_{ach} = 0.30\mu S$ between PNs and LNs where t_o is presynaptic firing time and t_delay is the axonal delay.

For GABAa-ergic synapses:

$$E_{GABAa} = 0mV,\ V_0 = -20mV,\ \sigma = 1.5,\ \alpha = 10ms^{-1},\ \beta = 0.16ms^{-1}$$

$$[T] = \frac{1}{1 + e^{-(V_{pre} - V_0)/\sigma}}$$

with $g_{GABAa} = 1.3\mu S$ between LNs and $g_{GABAa} = 0.8\mu S$ between LNs and PNs where V_{pre} is presynaptic membrane potential.

But the metabotropic GABAb receptors a more complex kinetics:

$$I_{GABAb} = g_{GABAb}\frac{[G]^4}{[G]^4 + K}(V - E_{GABAb})$$

$$\frac{d[G]}{dt} = r_3[R] - r_4[G]$$

$$\frac{d[R]}{dt} = r_1(1 - [R])[T] - r_2[R]$$

$$E_{GABAb} = -95mV,\ A = 0.5,\ t_{max} = 0.3ms,\ t_{delay} = 0.0$$

$$r_1 = 1mM^{-1}ms^{-1},\ r_2 = 0.01ms^{-1},\ r_3 = 0.1ms^{-1},\ r_4 = 0.06ms^{-1},\ K = 100\mu M^4$$

$$[T] = A\theta(t_{max} + t_o + t_{delay} - t)\theta(t - t_o - t_{delay}))$$

with $g_{GABAb} = 0.15\mu S$ between LNs and PNs where t_0 is presynaptic firing time.

Finally, if the presynaptic firing response from ORNs is $F(t)$, the stimulation current is:

$$I_{stim} = g_{max}F(t)(V - E_{ach})$$

We use TensorFlow to simulate the network of these neurons. [20]

KC-GGN model

In the final part of our simulation, to implement a vast number of neurons (15000 KCs) that lie postsynaptic to the PNs, we modeled them with a map-based Rulkov model[29, 30, 28, 1, 12, 31] since it is very computationally efficient. The KCs and the GGNs were modeled as regular spiking neurons and graded neurons, respectively, with the equations and parameters for KCs from Sanda et al. 2016[31].

The KCs were modelled as:

$$x_{n+1} = f_\alpha(x_n, x_{n+1}, y_n + \beta_n)$$

$$y_{n+1} = y_n - \mu(1 + x_n) + \mu(\sigma + \sigma_n)$$

with

$$f_\alpha(x_n, x_{n+1}, u) = \begin{cases} \alpha/(1 - x_n) + u & \text{if } x_n \leq 0 \\ \alpha + u & \text{if } 0 \leq x_n \leq \alpha + u \textit{ and } x_{n-1} \leq 0 \\ -1 & \text{otherwise} \end{cases}$$

where x_n is representative of membrane voltage at nth millisecond. For KCs, the parameter μ which affects the slow dynamics of the membrane was distributed $\sim 0.0012 + Uniform(-0.00068, 0.00068)$ which had been fit to match the population response of the cells, as recorded in vivo. To introduce variability in KCs, *sigma* was set to $0.06 + e$, where $e \sim Exponential(0.0072)$ The input variables were proportional to the injected current I, $\beta_n = I\beta_e$, $\sigma_n = I\sigma_e$, and the synaptic input β_n was limited to the range of $[-1, 1]$. The other parameters were set to $\alpha = 3.65$, $\beta_e = 0.03$, $\sigma_e = 1$. Initial conditions were set as $x_0 = x_1 = \sigma - 1, y_0 = x_0 - \alpha/(1 - x)$.

The GGN was modelled as:

$$x_{n+1} = \alpha f(x_n) - y_n$$
$$y_{n+1} = y_n - \mu(1 + x_n) + \mu(\sigma + \sigma_n)$$

with

$$f_\alpha(x_n) = \begin{cases} 2 & \text{if } x_n > 3 \\ x_n - \frac{x_n^3}{27} & \text{if } -3 \leq x_n \leq 3 \\ -2 & \text{otherwise} \end{cases}$$

where the parameters are $\alpha = 0.8, \mu = 0.005, \sigma = -0.5$ and initial conditions: $x_0 == \sigma - 1, y_0 = \alpha(x_0 - x_0^3/27) - x_0$.

In order to model the synaptic connections, we use a map-based Acetylcholine synapse and map-based GABAergic synapses. Excitatory synapses from PN to KC and KC to GGN are modelled as:

$$g_{n+1}^{syn} = \gamma g_n^{syn} + \begin{cases} G_{Ach}/S_{Dend} & \text{if presynaptic spike} \\ 0 & \text{otherwise} \end{cases}$$

$$I_n = \begin{cases} -g_n(x_n^{post} - E_{Ach}) & x_n^{post} - E_{Ach} < 0 \\ 0 & \text{otherwise} \end{cases}$$

x_n^{post} refers to x_n on the postsynaptic neuron. The presynaptic neuron is said to spike when it satisfies $x_n \geq \alpha + y_n + \beta_n$ or x_{n-1}. Here the parameters are set as $G_{ACh}(PN \to KC) = 0.00066$, $G_{ACh}(KC \to GGN) = 0.05$, the decay constant $\gamma = 0.4$, reversal potential $E_{ACh} = 0$, ratio between size of dendrite and some $S_{Dend} = 165 \times 10 - 6$. Similarly inhibitory synapses from GGN to KC follow:

$$g_{n+1}^{syn} = \gamma g_n^{syn} + \begin{cases} \frac{1}{1 + \frac{e^{\frac{-x_n^{pre}+1.5}{1.5}} G_{GABA}}{S_{Dend}}} & \text{if } x_n^{pre} > -1.4 \\ 0 & \text{otherwise} \end{cases}$$

$$I_n = -g_n(x_n^{post} - E_{GABA})$$

with maximum conductance G_{GABA} fixed to 0.00004 and $E_{GABA} = -0.7$. The connectivity is made such that $P(PN \to KC) = 0.3$ but all KCs converge onto the GGN and the GGN synapses back to all of the KCs.

4 Progress

During the last 1.5 months, the code for the model described above was implemented in Python 3.6. The implementation was done coherently by designing generator functions for three types of parameter files to maintain the same circuitry and experimental parameters across trials. These parameter files include a ".locust" file that generates a dictionary of the set of values drawn from the random distributions of each parameter that describe the whole circuitry and network parameters of a locust, the ".protocol" file that stores values pertaining to the structure of odor delivery experiment to any given locust, and a ".odor" file that determines the odor that was delivered to the Locust.

We use TensorFlow to implement the locust AL model based on PSST described in Mohanta et. al.[20] 2019. At the start of each trial, we select a ".locust," ".protocol," and ".odor" that runs a complete experiment and returns the neural output and input in each step. The code can be found under the "B.Model/Olfactory System" directory in the GitHub repository https://github.com/technosap/DAMN.

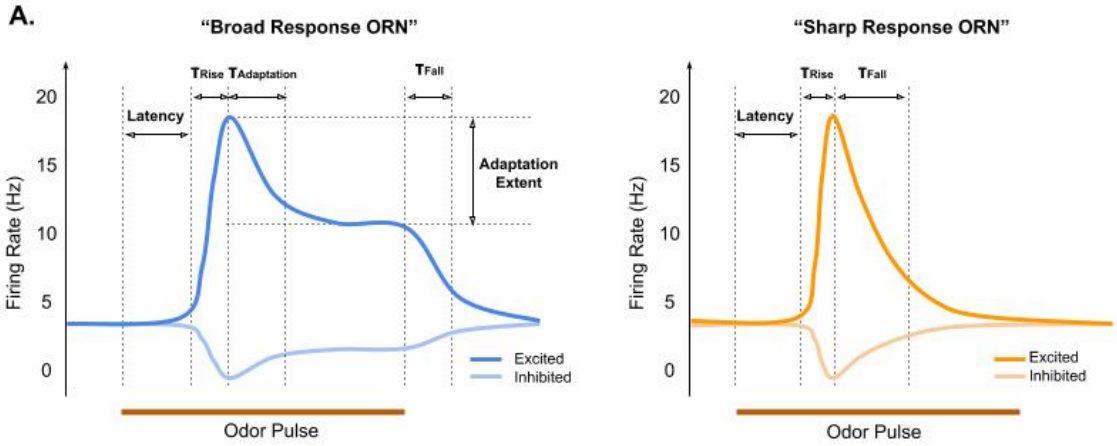
A.
"Broad Response ORN"
"Sharp Response ORN"
Latency
TRise
TAdaptation
TFall
Adaptation Extent
Firing Rate (Hz)
Excited
Inhibited
Odor Pulse

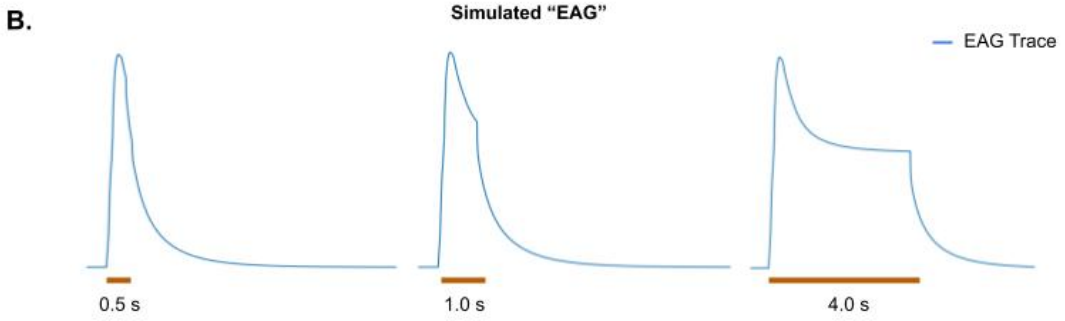
B.
Simulated "EAG"
EAG Trace
0.5 s
1.0 s
4.0 s

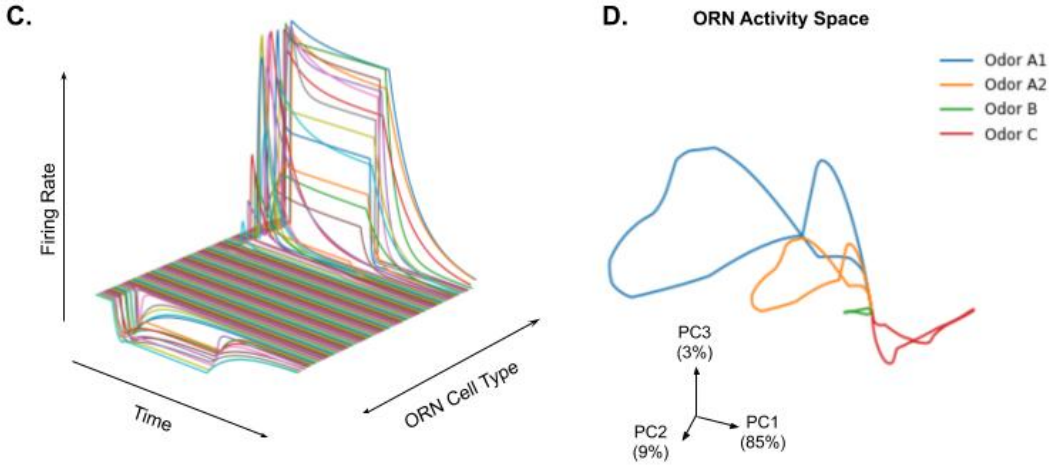
C.
Firing Rate
Time
ORN Cell Type
D.
ORN Activity Space
Odor A1
Odor A2
Odor B
Odor C
PC3 (3%)
PC2 (9%)
PC1 (85%)

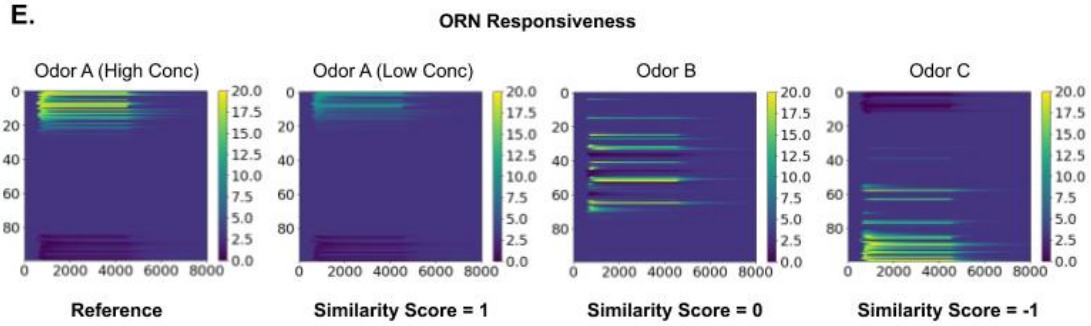
E.
ORN Responsiveness
Odor A (High Conc)
Odor A (Low Conc)
Odor B
Odor C
Reference
Similarity Score = 1
Similarity Score = 0
Similarity Score = -1

Figure 2: ORNs can be modelled using a firing rate model based on in-vivo experiments. (A) Classes of ORN behavior in response to Odorants and description of parameters. Some ORNs ("Sharp Response ORNs") show a sharp increase or decrease in activity and quickly return to the initial firing rate. A different class of ORNs shows an adapted response throughout the odor presentation (B) Simulated Electroantennogram (EAG) Data generated for 0.5 s, 1 s, and 4 s odor presentation by averaging ORN activity. This form is similar to experimental data in Sanda et al. 2016 (C) Diverse Responses of ORN cell types to odor presentation. Odor A1 refers to a high concentration of Odor A. Odor A2 refers to a low concentration of Odor A. (D) Representative odor trajectories in the ORN activity space (E) ORN responses to odors of varying concentrations and similarities. Similarity Score refers to cosine similarity.

4.1 ORN Model

A working model of the ORNs has been developed. The average response of the ORNs looks similar to in-vivo EAG recordings from Locust Antennas. (Fig 2.B) As predicted, a broad diversity of ORN input results in vast diversity in the input to the PNs in the antennal lobe. However, due to large arborization, the input to LNs are at a lot closer to the EAG form as predicted. It is found to be almost the same for all of the LNs and is also similar across odors. Thus, there is not a strong representation of odor identity in the LN input. The LN input does not have much variety, while the PNs have very diverse inputs that can encode odor identity. (Fig 3.B) We were also able to plot the trajectory of the system in 3-D space of the first three principal components of the population activity. (Fig 3.D)

However, this large arborization leads to another issue that may have a biological resolution but may appear as a drawback of our model. Since the ORNs have a baseline firing rate and the response to odor may be depolarization or hyperpolarization, the input from a large set of ORNs brings down the ratio of the baseline current to peak current during odor in the LNs. We refer to this as the systematic signal-to-noise ratio (systematic SNR). One cause of this is that we do not emulate the nonlinearities of dendritic integration and add the firing rates to build the AL input. This issue has somewhat been solved by having a conductance-based approach. The firing input is then scaled linearly to a suitable value for the conductance input for the antennal lobe neurons. For this, we normalize the peak value to 0.66 nS for PNs and 0.1 nS for LNs.

4.2 AL Model

Due to abundant publication errors in earlier literature, reproducing the results has not been a very successful process. We are still in the process of trying to determine the best values of parameters that give us realistic responses to odors. (Fig 3.C) In order to find reliable values of parameters for the AL network we looked for specific network properties which include 15-30 Hz LFP oscillation in the PNs, Broad increase in activity on odor onset, Broad increase in activity on odor offset, 10-40 Hz firing in active PNs during odor presentation and finally a fixed point representation in the PN activity space. These are all properties that have been observed in-vivo, and theoretical studies have replicated a large number of properties of the experimental data, we have found a regime in the parameter space where a significant fraction of the requirements are satisfied. These parameters are described in the Approach section. We are still looking for the exact set of parameters that give all aspects of the desired behavior based on the work by Laurent's group. All out analysis will be done of the response to three odorants: Odor A (Reference), Odor B (Similarity Score = 0.86) and Odor C (Similarity Score = -1.0)

We were able to observe the LFP due to the projection neurons of the AL (Fig 3.C). During the odor pulse, there is an oscillation in the range of 20-40 Hz is obtained. The frequency of this LFP Oscillation decreases in bursts rather than gradually, which would have been the case if it was the synaptic input adaptation that modulated the frequency of the LFP Oscillations. (Fig 3.C) We suspect that the bursts may be correlated with spontaneous decreases in LFP amplitude during the odor pulse.

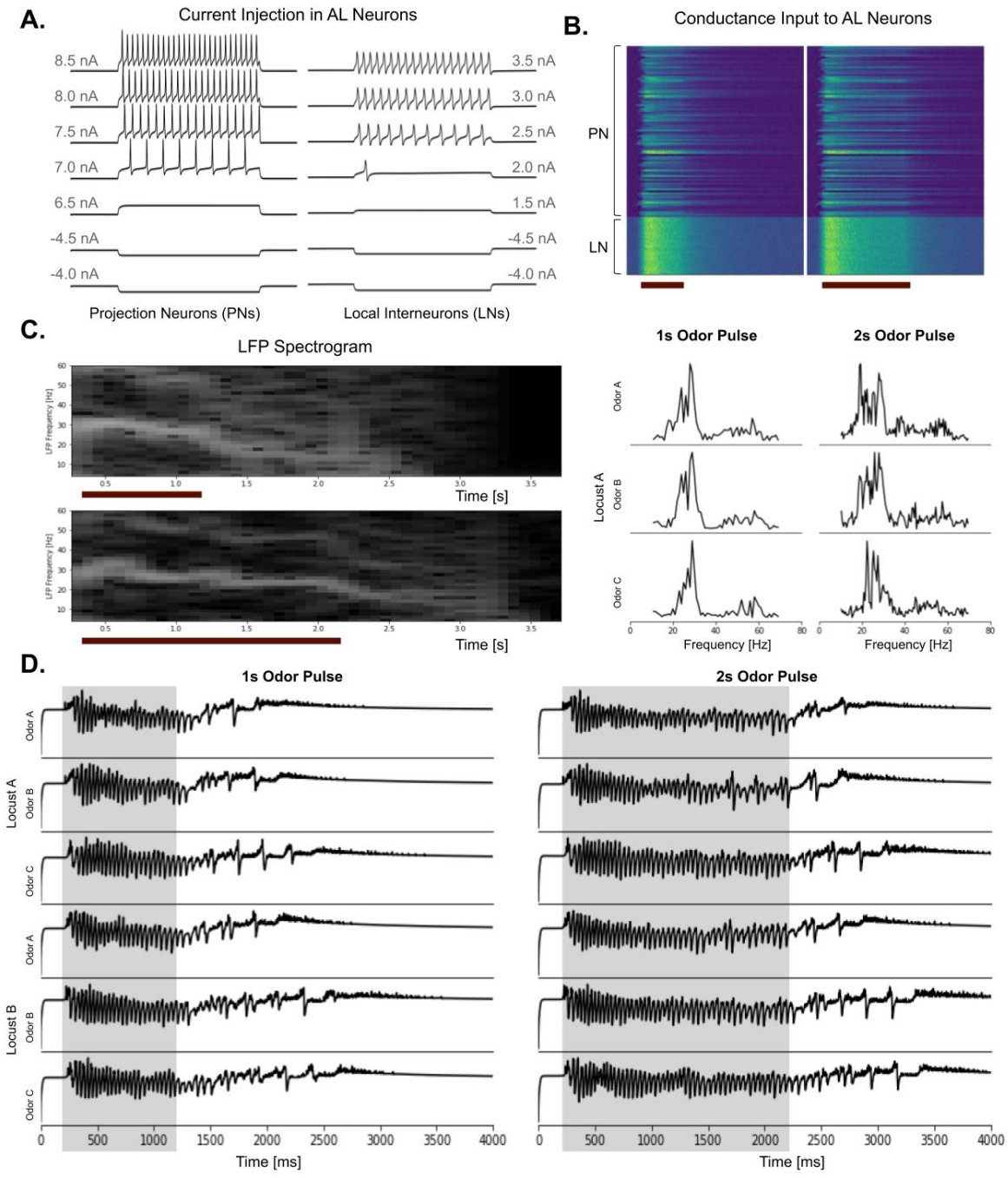

Figure 3: Isolated Neuron Properties are similar to in-vivo, and the neuronal population shows reliable population responses. (A) The response of synaptically isolated projection neurons (PNs) and local interneurons (LNs) to direct nano-current injection. (B) Max Peak Normalized Input to the 120 AL Neurons for the same odor for two different pulse durations. (C) Spectrogram and Fourier Spectra of the LFP due to PNs in the AL of the locust. (D) LFP Traces for two different Locusts in response to 3 different odors and two odor protocols. Single-trial data.

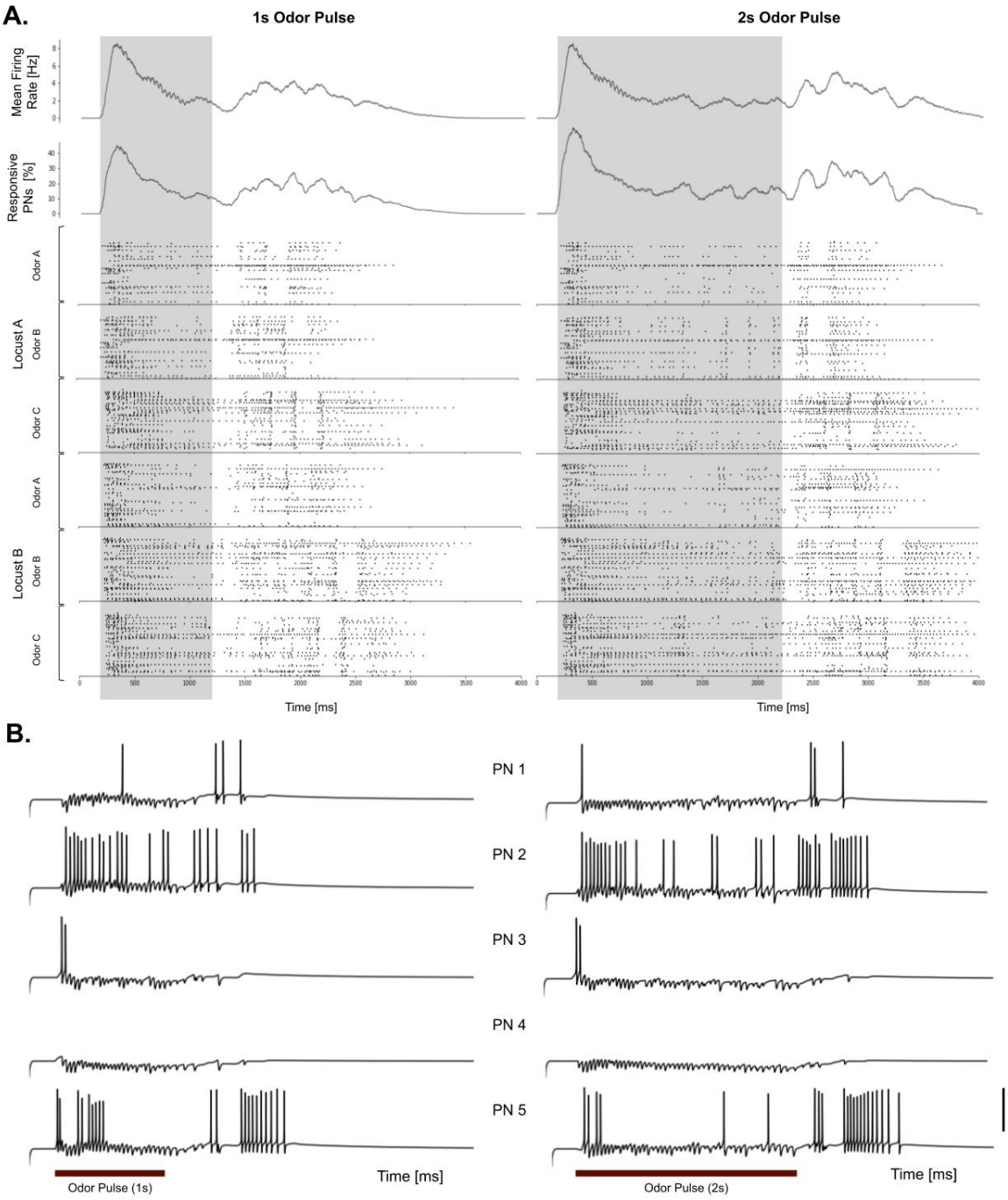

Figure 4: PNs respond to Odor Exposure in diverse forms as observed in-vivo with strong onset/offset activity and heavy tails. (A) Mean Firing Rate in 100 ms windows averaged over 90 PNs in a single trial for two artificial locusts and three odorants. The fraction of the PNs that are active in a 100 ms rolling window averaged for a single trial for two artificial locusts and three odorants. Raster-plots of the firing of the PN portrays the response of the PNs to diverse odorants in odor pulses of different length. Each dot signifies an action potential. (B) Diversity of PN responses to the odorant. The new model for AL input offers a more diverse and visibly more realistic diversity of responses in the PNs. Scale bar (right): 50 mV

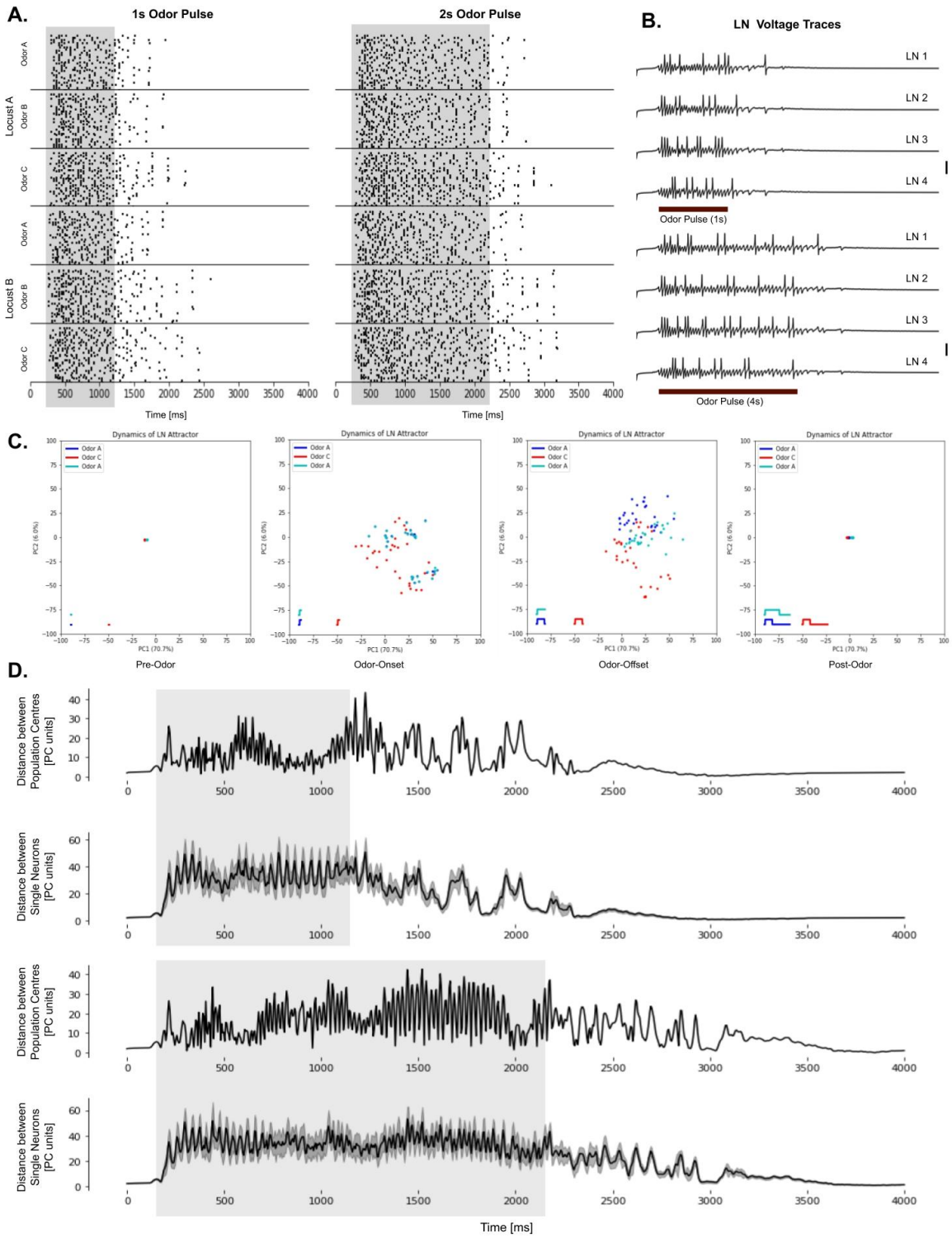

Figure 5: LNs can encode dynamic attractors in the population discriminate odors. (A) The response of LNs to diverse odorants. Each dot signifies an action potential. Scale bar (right): 30 mV. (B) Voltage traces for LNs on exposure to different duration of odor input. (C) Dynamics of LNs populations over time observed in the PC space of LN activity. (D) Distances between population centers of different odorants and mean distance of individual neuron responses between different odorants in different odor pulse protocols.

We find that by having a high (1.3 nS) GABAa conductance, we were able to improve synchrony and improve LFP power. We also saw that the ability of the neuronal population to generate an LFP is very reliable across odorants, animals, and timescales. (Fig 3.D) In order to attain a temporal patterning other than just switching, we set up a slow GABAb current. We observed that increasing the rate of the offset of GABAb receptors allowed us to have diverse patterns such as temporary silencing, onset/offset firing, and heavy-tailed responses, which have not been extensively described in earlier computational studies. (Fig 4.A, B) We were able to replicate specific results obtained experimentally by Laurent's group. We see an offset increase in both mean firing rate and percentage of responsive neurons, but in the experiments, the offset responses are stronger than onset responses, which we do not find in our parameter regime. Also, both mean firing rate and percentage of responsive neurons show almost double the activity than what is observed in-vivo. These issues can be corrected by using lower conductances. However, the fast offset of GABAb has led to the increased synchronous firing, which is not generally observed in-vivo. By tweaking the offset timescales of GABAb, we should be able to find a regime of stable heavy tails.

A quick look at the LN responses tells us that almost all LNs show some activity. This response, which has been observed in-vivo, is present in all individuals in response to all odorants. (Fig 5. A) None of the LNs remain constitutively on/off, unlike previous models. However, we do observe switching-like behavior between LNs in short time windows. (Fig 5. B) In order to study attractor dynamics in the LNs, we train a Principal Component Analysis (PCA) model in which fit 100ms long slices of single LN dynamics to create a lower-dimensional space (2D) of LN activity. (Fig 5. C) Each point in this 2D-PCA space represents the activity of a single LN. We found that on training with every fifth 100ms window from 2 locusts, three odorants, and two protocols (with one trial each), the first PC could explain 70.7% of the variance while the second explained 6%. The population response at any 100ms interval can be given by and arrangement of 30 points (local interneurons) in the 2D-PC space. As the odor progresses, the points will move in the 2D space. The differences in the trajectories are what will allow us to discriminate between odors. Dynamics of Population and Individuals Neural Responses can be determined by looking at the distance between population centers for two odors in the same odor delivery protocol and the distances between the neural representation of different odors in the same neuron. (Fig 5. D) The data from a single trial shows that the distance between centroids of two different odors is not consistently maintained in this model of attractor systems. There are times when the network separates the odor centroids, particularly at the offset of odor. Averaging over more trials will solidify this hypothesis and help us identify attractor states that are representative of the odor. Nevertheless, we can see that despite oscillations, on average, individual neurons subject to different odors do maintain distance between their representations in PC space. Thus individual activity can help us discriminate between odors.

4.3 KC-GNN model

A working map-based KC-GGN model has been implemented that can take the output from the AL simulation and use it to simulate the activity of the MB in the presence of dynamic feedback inhibition by the GGN.(Fig 6.C,D) The large arborization of KCs in Locusts giving them a significant fraction of input (Fig 6.A) can theoretically improve the number of odors that can be represented combinatorially in the MB, but broad activation in the PNs may fail to drive unique and robust activation of the KCs and thus cannot efficiently code the odor identity. Especially in such cases, it is suggestive that the GGN pruning the KC activity is essential for reliable odor identity representation. We generate a 20 Hz input with only 10% of PNs (Fig 6.B) and observe an enormous number of spikes in the MB, which gradually die down and leading to a sparser representation (Fig 6. C.ii) by active regulation by GGN (Fig 6.C.iii). In order to see how the GGN was important, we artificially "ablate" or remove the GGN-KC synapse and run the same simulation (Fig 6.D.i), and we find that the representation is much denser. (Fig 6.D.ii) Thus, it is clear that the GGN plays a huge role, and since there is a lag before which the system is sparse enough to have a reliable but unique representation, the GGN is going to play a huge role in the representation of AL dynamics in the MB.

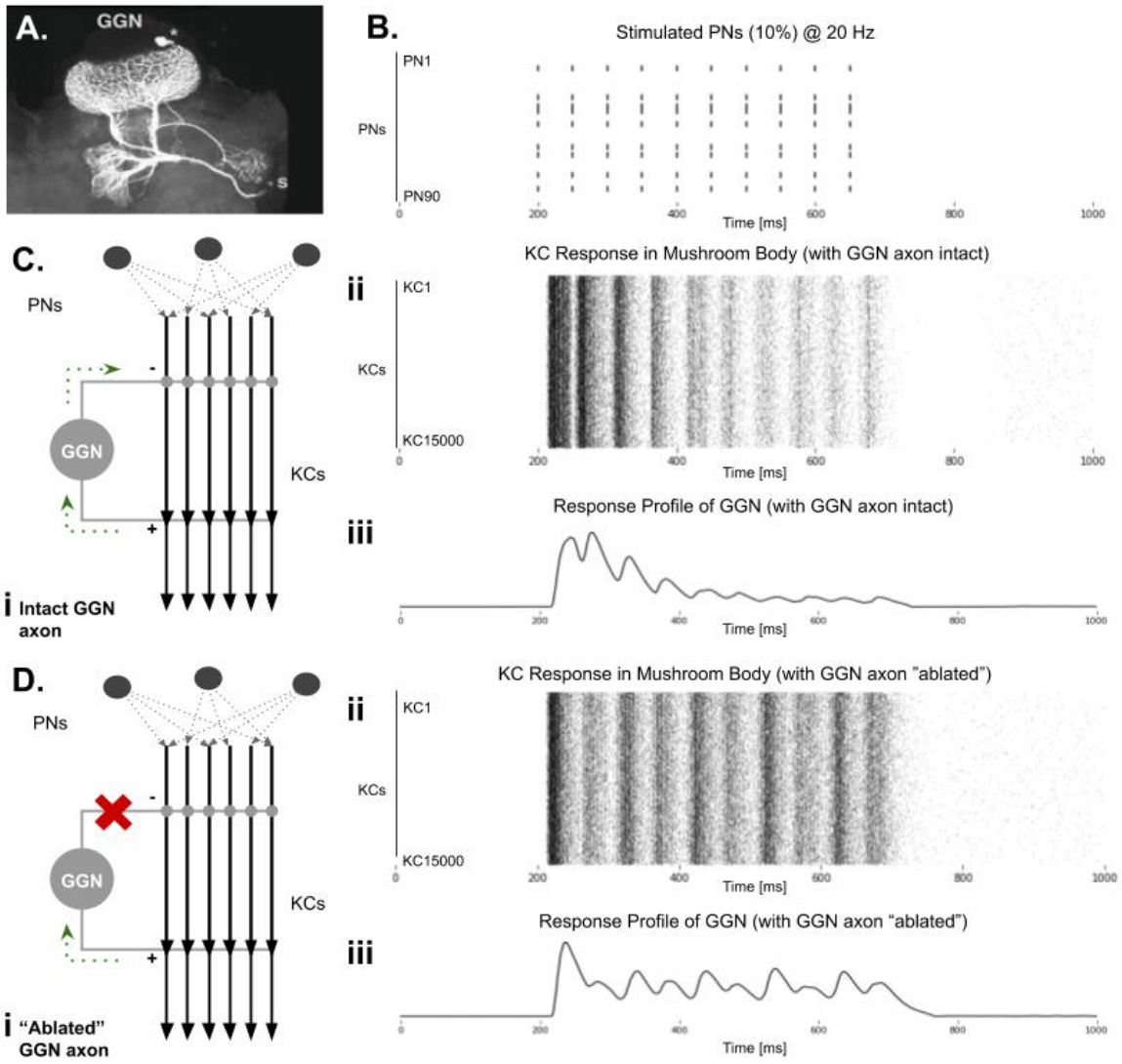

Figure 6: The KC-GGN model can actively sparsify the mushroom body response to odors. (A) Morphology of the GGN in Locust with extensive arborization in the MC calyx, alpha lobe, and the lateral horn (LH) (B) Uniform 20 Hz stimulation of 10% of PNs in the AL to excite the KCs in the MB (C) i. Schematic of the KC-GGN circuitry with all connections intact, leading to negative feedback. ii. Gradually sparsification of KC firing in the presence of the GGN. iii. Initially, the GGN is highly active, but the reduction in KC activity reduces GGN activity. (D) i. Schematic of the KC-GGN circuitry with the GGN-KC axon ablated removing the negative feedback. ii. Irregular and Dense KC firing on the ablation of the GGN. iii. The GGN continues to be highly active as there is no reduction in KC.

5 Conclusion

This project is progressing steadily. We have found some values in the parameter space that can give us quite realistic responses in PNs, and the code can be run very smoothly to simulate a broad spectrum of experiments designed much like experimental paradigms. Currently, we do not have enough replicates to analyze fixed points. However, once we have the data, it can be analyzed by looking at PC trajectories in the activity space and characterizing the properties of the trajectory such as velocity with time, the distance between odors with time, residence timings at a fixed point and other PC space analysis. In order to confirm our hypothesis, we need to show community structures in LN space and how it links with the random structure of the LN network and the entrainment of the PN population by the LN population. We can also check if the switches in the community are linked with abrupt changes in LFP amplitude and frequency. Once we have a fully functional system, a lot of other questions can also be asked simultaneously, such as the transfer of relevant odor information across levels of the Locust olfactory system and the importance of feedback from GGN in this process.

References

[1] Collins Assisi, Mark Stopfer, Gilles Laurent, and Maxim Bazhenov. Adaptive regulation of sparseness by feedforward inhibition. *Nature neuroscience*, 10(9):1176, 2007.

[2] Richard Axel. The molecular logic of smell. *Scientific American*, 273(4):154–159, 1995.

[3] Maxim Bazhenov, Mark Stopfer, Mikhail Rabinovich, Henry DI Abarbanel, Terrence J Sejnowski, and Gilles Laurent. Model of cellular and network mechanisms for odor-evoked temporal patterning in the locust antennal lobe. *Neuron*, 30(2):569–581, 2001.

[4] Maxim Bazhenov, Mark Stopfer, Mikhail Rabinovich, Ramon Huerta, Henry DI Abarbanel, Terrence J Sejnowski, and Gilles Laurent. Model of transient oscillatory synchronization in the locust antennal lobe. *Neuron*, 30(2):553–567, 2001.

[5] Allison F Carey and John R Carlson. Insect olfaction from model systems to disease control. *Proceedings of the National Academy of Sciences*, 108(32):12987–12995, 2011.

[6] P Duchamp-Viret, B Palouzier-Paulignan, and A Duchamp. Odor coding properties of frog olfactory cortical neurons. *Neuroscience*, 74(3):885–895, 1996.

[7] Catherine Dulac. How does the brain smell? *Neuron*, 19(3):477–480, 1997.

[8] Shabnam Sarah Farivar. *Cytoarchitecture of the locust olfactory system*. PhD thesis, California Institute of Technology, 2005.

[9] C Giovanni Galizia. Olfactory coding in the insect brain: data and conjectures. *European Journal of Neuroscience*, 39(11):1784–1795, 2014.

[10] Elissa A Hallem and John R Carlson. Coding of odors by a receptor repertoire. *Cell*, 125(1):143–160, 2006.

[11] Seth Haney, Debajit Saha, Baranidharan Raman, and Maxim Bazhenov. Differential effects of adaptation on odor discrimination. *Journal of neurophysiology*, 120(1):171–185, 2018.

[12] Tiffany Kee, Pavel Sanda, Nitin Gupta, Mark Stopfer, and Maxim Bazhenov. Feed-forward versus feedback inhibition in a basic olfactory circuit. *PLoS computational biology*, 11(10):e1004531, 2015.

[13] Gilles Laurent. Dynamical representation of odors by oscillating and evolving neural assemblies. *Trends in neurosciences*, 19(11):489–496, 1996.

[14] Gilles Laurent. A systems perspective on early olfactory coding. *Science*, 286(5440):723–728, 1999.

[15] Beulah Leitch and Gilles Laurent. Gabaergic synapses in the antennal lobe and mushroom body of the locust olfactory system. *Journal of comparative Neurology*, 372(4):487–514, 1996.

[16] Hongwei Li, Peng Wang, Liwei Zhang, Xiao Xu, Zewen Cao, and Long Zhang. Expressions of olfactory proteins in locust olfactory organs and a palp odorant receptor involved in plant aldehydes detection. *Frontiers in physiology*, 9:663, 2018.

[17] Katrina MacLeod and Gilles Laurent. Distinct mechanisms for synchronization and temporal patterning of odor-encoding neural assemblies. *Science*, 274(5289):976–979, 1996.

[18] Joshua P Martin, Aaron Beyerlein, Andrew M Dacks, Carolina E Reisenman, Jeffrey A Riffell, Hong Lei, and John G Hildebrand. The neurobiology of insect olfaction: sensory processing in a comparative context. *Progress in neurobiology*, 95(3):427–447, 2011.

[19] Ofer Mazor and Gilles Laurent. Transient dynamics versus fixed points in odor representations by locust antennal lobe projection neurons. *Neuron*, 48(4):661–673, 2005.

[20] Saptarshi Soham Mohanta and Collins Assisi. Parallel scalable simulations of biological neural networks using tensorflow: A beginner's guide. *arXiv preprint arXiv:1906.03958*, 2019.

[21] Bruno A Olshausen and David J Field. Sparse coding of sensory inputs. *Current opinion in neurobiology*, 14(4):481–487, 2004.

[22] Mainak Patel, Aaditya V Rangan, and David Cai. A large-scale model of the locust antennal lobe. *Journal of computational neuroscience*, 27(3):553–567, 2009.

[23] Javier Perez-Orive, Maxim Bazhenov, and Gilles Laurent. Intrinsic and circuit properties favor coincidence detection for decoding oscillatory input. *Journal of Neuroscience*, 24(26):6037–6047, 2004.

[24] Javier Perez-Orive, Ofer Mazor, Glenn C Turner, Stijn Cassenaer, Rachel I Wilson, and Gilles Laurent. Oscillations and sparsening of odor representations in the mushroom body. *Science*, 297(5580):359–365, 2002.

[25] Baranidharan Raman, Joby Joseph, Jeff Tang, and Mark Stopfer. Temporally diverse firing patterns in olfactory receptor neurons underlie spatiotemporal neural codes for odors. *Journal of Neuroscience*, 30(6):1994–2006, 2010.

[26] Baranidharan Raman, Ping A Sun, Agustin Gutierrez-Galvez, and Ricardo Gutierrez-Osuna. Processing of chemical sensor arrays with a biologically inspired model of olfactory coding. *IEEE Trans. Neural Networks*, 17(4):1015–1024, 2006.

[27] Michel Renou. Pheromones and general odor perception in insects. *Neurobiology of chemical communication*, page 23, 2014.

[28] Nikolai F Rulkov. Modeling of spiking-bursting neural behavior using two-dimensional map. *Physical Review E*, 65(4):041922, 2002.

[29] Nikolai F Rulkov and Maxim Bazhenov. Oscillations and synchrony in large-scale cortical network models. *Journal of biological physics*, 34(3-4):279, 2008.

[30] Nikolai F Rulkov, Igor Timofeev, and Maxim Bazhenov. Oscillations in large-scale cortical networks: map-based model. *Journal of computational neuroscience*, 17(2):203–223, 2004.

[31] Pavel Sanda, Tiffany Kee, Nitin Gupta, Mark Stopfer, and Maxim Bazhenov. Classification of odorants across layers in locust olfactory pathway. *Journal of neurophysiology*, 115(5):2303–2316, 2016.

[32] Mark Stopfer, Vivek Jayaraman, and Gilles Laurent. Intensity versus identity coding in an olfactory system. *Neuron*, 39(6):991–1004, 2003.

[33] Rufin VanRullen, Rudy Guyonneau, and Simon J Thorpe. Spike times make sense. *Trends in neurosciences*, 28(1):1–4, 2005.

[34] R Hamilton Wright, JR Hughes, and DE Hendrix. Olfactory coding. *Nature*, 216(5113):404, 1967.